Fermi arcs and surface criticality in dirty Dirac materials

Eric Brillaux and Andrei A. Fedorenko

Université de Lyon, ENS de Lyon, Université Claude Bernard, CNRS, Laboratoire de Physique, F-69342 Lyon, France

We study the effects of disorder on semi-infinite Weyl and Dirac semimetals where the presence of a boundary leads to the formation of either Fermi arcs/rays or Dirac surface states. Using a local version of the self-consistent Born approximation, we calculate the profile of the local density of states and the surface group velocity. This allows us to explore the full phase diagram as a function of boundary conditions and disorder strength. While in all cases we recover the sharp criticality in the bulk, we unveil a critical behavior at the surface of Dirac semimetals, which is smoothed out by Fermi arcs in Weyl semimetals.

Introduction. Three-dimensional nodal semimetals are materials where several energy bands cross linearly at isolated points in the Brillouin zone: two bands in Weyl semimetals [1,2] and four bands in Dirac semimetals [3–5]. They exhibit remarkable phenomena related to the relativistic nature of the low-energy excitations and topological properties of the band structure [6–9]. In particular, the bulk-boundary correspondence leads in Weyl semimetals to topologically protected surface-localized states in the form of Fermi arcs that connect the surface projections of Weyl nodes with opposite chirality [10–12]. They have been observed using photoemission spectroscopy in inversion-symmetry-breaking crystals such as tantalum arsenide (TaAs) [1,13] and niobium arsenide (NbAs) [2], where their shape and topological properties agree beautifully with first-principles calculations [14]. In Dirac semimetals, scattering from the boundary can also produce propagating surface modes with energies near the bulk band crossing which, however, are not topologically protected [8]. Experimentally, Dirac semimetals host at least one pair of Dirac nodes (like in Na_3Bi), so that the Fermi surface may consist of two arcs that bridge the two bulk nodes [15]. The local properties of the emergent surface states are controlled by the boundary conditions, which describe how the different degrees of freedom such as pseudospin and valley index mix upon quasiparticle reflection from the surface [16–18].

The presence of disorder such as lattice defects or impurities can strongly modify the behavior of clean materials, or even lead to quantum phase transitions such as Anderson localization [19]. A new type of disorder-induced quantum phase transition was recently discovered in relativistic semimetals [20,21], wherein a strong enough disorder drives the semimetal towards a diffusive metal. Inside the bulk, the average density of states (DOS) at the nodal point plays the role of an order parameter since it becomes nonzero above a critical disorder strength [20,22–29]. This bulk transition has been intensively studied using both numerical simulations [30–35] and analytical methods [36–42]. The effects of rare events have also been much debated [43–52].

How disorder affects the surface states of relativistic semimetals is much less known. Perturbative calculations show that the surface states in generic Dirac materials are protected from surface disorder due to their extension far into the bulk, which reduces the overlap with impurities [16]. Numerical simulations also indicate that while Fermi arcs in Weyl semimetals are robust against weak bulk disorder, they hybridize with nonperturbative bulk rare states as the strength of disorder gradually increases and completely dissolve into the emerging metallic bath at the bulk transition [49,53].

In this Letter, we study the effect of weak disorder on the surface states produced by generic boundary conditions in a minimal model for both Weyl and Dirac semimetals. We develop a local version of the self-consistent Born approximation (SCBA) [42] to compute the DOS profile and the surface group velocity as a function of disorder strength. While the SCBA is poorly controlled close to the transition and fails to produce the exact critical exponents, it still enables one to capture the qualitative behavior of various observables [54]. In particular, we investigate the full phase diagram in the presence of a surface and show that it bears similarities with that of semi-infinite magnetic systems, which exhibit ordinary, surface, and extraordinary phase transitions [55,56]. We find that a boundary of a nodal semimetal that hosts Dirac surface states turns into a metallic state at a critical disorder strength lower than that in the bulk. Upon further increasing disorder, the bulk becomes metallic in the presence of the metallic surface, thus experiencing an extraordinary transition. Yet, in the Weyl semimetals, the surface states from the Fermi arcs smooth out surface criticality.

Boundary conditions for a semi-infinite semimetal. The Nielsen-Ninomiya theorem constrains relativistic semimetals to host pairs of nodes with opposite Berry charges [57]. A minimal low-energy theory for such materials thus comprises two Weyl nodes of opposite chiralities, separated in the Brillouin zone by a momentum $2\boldsymbol{b}$. Below a suitable cutoff momentum Λ, the quasiparticles are determined by the binodal Weyl Hamiltonian [29],

$$H_0 = i\tau_z \boldsymbol{\sigma} \cdot \boldsymbol{\partial} + \tau_0 \boldsymbol{\sigma} \cdot \boldsymbol{b}, \tag{1}$$

where $\boldsymbol{\partial} = (\partial_x, \partial_y, \partial_z)$ denotes the gradient operator. In Eq. (1), we use the Pauli matrices $\boldsymbol{\sigma} = (\sigma_x, \sigma_y, \sigma_z)$ and
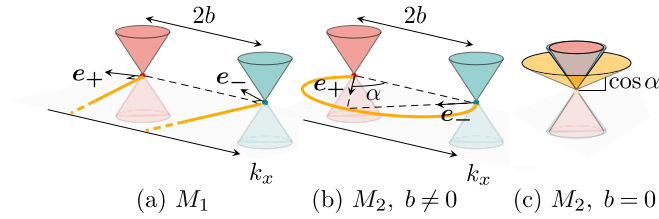
FIG. 1. Projection to the surface Brillouin zone (k_x, k_y) of bulk Weyl cones with chiralities $+1$ (red) and -1 (blue). Surface states disperse along lines at the Fermi level (orange). (a) Fermi rays oriented by the vectors $e_\pm$. (b) Fermi arc with curvature α. (c) Surface cone with Fermi velocity $\cos\alpha$.

(τ_x, τ_y, τ_z) for the pseudospin and valley—or chiral—degrees of freedom, respectively. The identity matrices are denoted as σ_0, τ_0. We can formally tune $\boldsymbol{b}$ to describe either a pair of Weyl cones ($\boldsymbol{b}$ arbitrary) or a single Dirac cone ($\boldsymbol{b} = \boldsymbol{0}$) when additional spatial symmetries prevent the nodes from hybridizing and opening a gap.

In a semi-infinite material filling the $z \geqslant 0$ half space, we must supplement the bulk Hamiltonian (1) with proper boundary conditions (BCs) at the surface. Assuming a generic BC that can describe not only a free surface, but also a surface that is covered by various chemical layers, we impose

$$M\psi|_{z=0^+} = \psi|_{z=0^+}, \quad (2)$$

where the unitary Hermitian matrix M ensures the nullity of the transverse current: $\{M, \tau_z\sigma_z\} = 0$ [17,18]. Two classes of matrices satisfy these criteria. They are both parametrized by a pair of angles (θ_+, θ_-) such that

$$M_1 = \tau_+(\boldsymbol{\sigma} \cdot \boldsymbol{e_+}) + \tau_-(\boldsymbol{\sigma} \cdot \boldsymbol{e_-}), \quad (3a)$$

$$M_2 = (\boldsymbol{\tau} \cdot \boldsymbol{e_+})\sigma_+ + (\boldsymbol{\tau} \cdot \boldsymbol{e_-})\sigma_-, \quad (3b)$$

where $\boldsymbol{e_\pm} = (\cos\theta_\pm, \sin\theta_\pm, 0)$ are two unitary vectors of the surface, and $\mu_\pm = (\mu_x \pm i\mu_y)/2$ with $\mu = \tau, \sigma$ are the chiral and pseudospin projectors.

The BC 3(a) describes Weyl fermions that retain the same chirality under scattering from the boundary. The emerging surface states at the Fermi level distribute along two independent Fermi rays pointing in the directions orthogonal to $\boldsymbol{e_\chi}$, stemming from the nodes of topological charges $\chi = \pm 1$, respectively, regardless of the distance between the nodes, as illustrated in Fig. 1(a) (see the Supplemental Material [58]). This BC breaks the O(2) rotational symmetry in the (x, y) plane by imposing the rays' orientations, which must be determined by microscopic details of the boundary, and thus should be extremely sensitive to surface roughness [59]. It also mixes neighboring Landau levels in a background magnetic field, making Landau quantization ill defined [60]. Seemingly infinite Fermi rays extend to the full Brillouin zone and thus could terminate at another remote pair of Weyl nodes [17].

The BC 3(b), on the contrary, mixes chirality of reflected quasiparticles, and thus depends on the relative positions of the Weyl nodes. Without loss of generality, we align the nodes in the x direction and set $\boldsymbol{b} = b\boldsymbol{e_x} + b_z\boldsymbol{e_z}$. (i) For a nonzero half separation b between the surface projections of the nodes, the surface states at the Fermi level disperse along a curved Fermi arc. Its parametric equation reads $\phi_+ - \phi_- + \theta_+ - \theta_- = 0$,

where ϕ_χ is the angle formed by the momentum measured from the node of chirality χ with the x axis. This defines a circular arc with aperture angle 4α and perimeter $L_{\mathrm{FA}} = 4b\alpha/\sin(2\alpha)$, as shown in Fig. 1(b), where the angle $\alpha = (\pi + \theta_+ - \theta_-)/2 \in [0, \pi/2]$ reduces here to θ_+ due to the alignment of the nodes along the x axis (see the Supplemental Material [58]). In experiments [13,61,62], Fermi arcs are usually distorted because of higher-order corrections to the linear dispersion relation. They can join two Weyl nodes (our model) but also two Dirac nodes or surface-projected nodes with higher topological charges, in which case multiple arcs are attached to the pair. (ii) When $b = 0$, the surface states are nontopological and form a single cone with Fermi velocity $v_0 = \cos\alpha$ that extends in either the electron or hole side, depending on the direction of the normal to the surface [16]. In our case, this corresponds to the positive energies, as shown in Fig. 1(c). This electron-hole surface asymmetry persists in the presence of a magnetic field or a gap, where the dispersion relation also depends on the extra parameter $\theta_\tau = (\theta_+ + \theta_-)/2$ [16]. Note that Fermi rays and arcs give rise to a nonzero surface DOS at all energies, while the density of the Dirac surface states shown in Fig. 1(c) vanishes at the nodal energy.

Treatment of disorder. Pointlike impurities generate disorder that is insensitive to the chiral and pseudospin degrees of freedom. Assuming the density of impurities is uniform in the bulk, we model such defects by a random, scalar, Gaussian potential $V(\boldsymbol{r})$ with zero average and short-range variance $\gamma\delta(\boldsymbol{r})$. In an infinite sample, disorder induces a second-order transition towards a diffusive metal phase above a nonzero critical value γ^*, though the critical point is probably avoided due to rare events [43–52]. The bulk average DOS $\bar{\rho}_b$, which vanishes on the semimetal side, increases in a power-law fashion, $\bar{\rho}_b \sim (\gamma - \gamma^*)^\beta$, above the critical point [20,22–29]. As shown below, the spatially resolved DOS reveals this behavior for all BC, but also a new surface transition in a single Dirac cone.

Local self-consistent Born approximation. The boundary breaks translational invariance along the perpendicular direction. Consequently, the retarded Green's function of the clean system, $G_0(\epsilon, z, z')$, depends not only on the distance $z - z'$ between the points, but also on the absolute distance $z + z'$ to the surface. It satisfies the boundary condition $MG_0(\epsilon, 0, z') = G_0(\epsilon, 0, z')$. Notice that we omit the explicit dependence on the momentum k parallel to the boundary for the sake of brevity. Introducing the disorder-averaged Green's function $G(\epsilon, z, z')$, which satisfies the same boundary condition, we define the corresponding self-energy Σ as

$$\{H_0 - [\epsilon + \Sigma(\epsilon, z)]\tau_0\sigma_0\}G(\epsilon, z, z') = \delta(z - z')\tau_0\sigma_0. \quad (4)$$

Within the SCBA and for pointlike disorder, the self-energy Σ is momentum independent in the bulk and proportional to the unit matrix [42]. In the absence of translational invariance, it is a function of z and satisfies the self-consistency equation

$$\Sigma(\epsilon, z) = \frac{\gamma}{4} \int_{|\boldsymbol{k}|<\Lambda} \frac{d^2k}{(2\pi)^2} \mathrm{Tr}[G(\epsilon, z, z)]. \quad (5)$$

The solution to Eqs. (4) and (5), where the latter relates the self-energy at position z to its values at all points, requires the
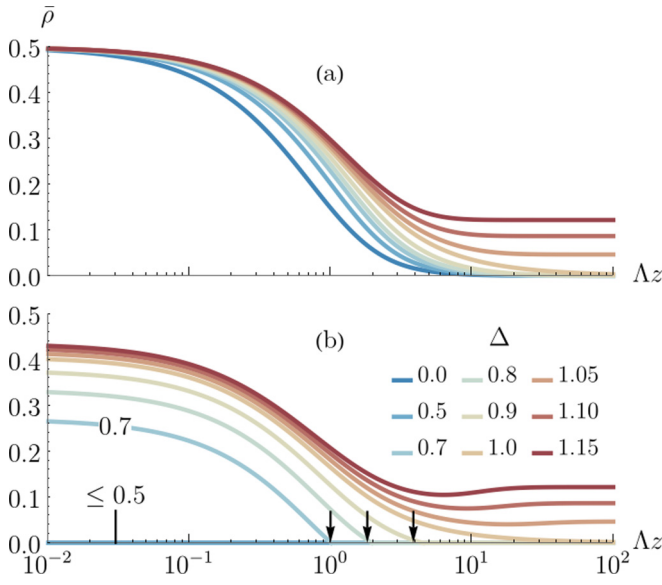
FIG. 2. LDOS profile for various disorder strengths Δ. The bulk density increases as $\frac{1}{2}(1 - \Delta^{-2})$ above the critical value $\Delta_b^* = 1$, and vanishes below. (a) Fermi rays (M_1 BC). (b) Dirac surface states (M_2 BC) with $\alpha = \pi/4$. $\bar{\rho}(z)$ vanishes everywhere for Δ smaller than the surface critical value, $\Delta_s^* = \cos(\alpha) = 0.5$. The arrows indicate the penetration length $\xi(\Delta)$, which diverges for $\Delta = 1$.

inversion of a non-translationally invariant Green's function. The problem is greatly simplified if one assumes that the spatial variations of the self-energy are small, i.e., if $\partial\Sigma/\partial z \ll (\epsilon + \Sigma)^2$ (see the Supplemental Material [58]). In this approximation, we replace $G(\epsilon, z, z)$ with $G_0[\epsilon + \Sigma(\epsilon, z), z, z]$ in Eq. (5) so that the self-energy now satisfies a self-consistency equation in which both sides involve $\Sigma(\epsilon, z)$ at the *same* position z. We refer to this scheme as the local self-consistent Born approximation (LSCBA).

In the presence of disorder, the surface band crossing arising from the M_2 BC is shifted from the bulk nodal energy [63] by $-\mathrm{Re}\Sigma(\epsilon, z)$. In this case, it is natural to calculate the density profile, not at a fixed chemical potential, e.g., at the bulk Fermi level, but at the energy of the local density minimum, $\epsilon_F(z) = -\mathrm{Re}\Sigma[\epsilon_F(z), z]$. This allows one to probe the band crossing structure close to the surface as a function of the distance to the surface and strength of disorder. To that end, we introduce the disorder-induced broadening $\Gamma > 0$ as $\epsilon_F(z) + \Sigma[\epsilon_F(z), z] = i\Gamma(z)$, from which we extract the minimum of the average LDOS at position z. The LDOS is given by $\bar{\rho} = (\mathrm{Tr}\,\mathrm{Im}\,G)/\pi$. Using the self-consistency equation (5), it can be rewritten in natural units as

$$\bar{\rho}(z) = \frac{4\pi\,\mathrm{Im}\,\Sigma[\epsilon_F(z), z]}{\gamma\Lambda^2} = \frac{\Gamma(z)}{\Delta\Lambda}, \tag{6}$$

where $\Delta = \gamma\Lambda/4\pi$ is the dimensionless disorder strength.

Effect of disorder on Dirac surface states. Let us focus first on the case $b = 0$. Using the LSCBA (5), we calculate the self-energy for both BCs leading either to Fermi rays for M_1 or to Dirac surface states for M_2. The corresponding LDOS profiles computed using Eq. (6) are depicted in Fig. 2(a) for Fermi rays, and in Fig. 2(b) for Dirac surface states with $\alpha = \pi/4$. For both BCs, we recover the bulk transition for

infinite z and at the critical disorder strength $\Delta_b^* = 1$, above which the LDOS behaves as $\bar{\rho}_b = \frac{1}{2}(1 - \Delta^{-2}) \propto |\Delta - \Delta_b^*|^\beta$ with $\beta = 1$. Below this critical value, the LDOS vanishes, as in infinite systems within the SCBA [42]. Exactly at criticality, the LDOS profile decreases algebraically as $(\Lambda z)^{-1}$.

Near the surface, however, the LDOS behaves very differently depending on the BC. For Fermi rays, disorder does not impact the density close to the boundary, which remains always finite since the rays pass through the whole Brillouin zone [see Fig. 1(a)]. The surface modes populating the rays propagate diffusively with a decreasing mean free path $l = 2/\Delta$ as we gradually increase the disorder strength, and dissolve into the metallic bulk above the semimetal-metal critical point.

On the contrary, as seen in Fig. 2(b), the local density of Dirac surface states vanishes above a distance $\Lambda z = \xi$ from the boundary, such that

$$\frac{1 - e^{-2\xi}}{2\xi} = \frac{\Delta^{-1} - 1}{(\tan\alpha)^2}. \tag{7}$$

Hence, Dirac surface states extend into the bulk over this penetration length ξ; they spread maximally at bulk criticality where it diverges like $\xi \sim |\Delta - \Delta_b^*|^{-\nu}$ with $\nu = 1$, which can be identified with the correlation length exponent.

Indeed, the values of the exponents β and ν agree with the mean-field values of the critical exponents for the order parameter and correlation length at the three-dimensional (3D) semimetal-diffusive metal transition computed within the SCBA [42]. In addition, both ξ and the LDOS vanish at the disorder strength $\Delta_s^* = (\cos\alpha)^2 < \Delta_b^*$, which shows that a surface transition takes place at Δ_s^*.

Before we consider the full phase diagram, let us discuss the validity of the LSCBA. The local approximation is justified when the derivative of $\Gamma(z)$ is small with respect to $\Gamma(z)^2$, which is satisfied close to the surface and deep in the bulk. It breaks down at intermediate distance to the boundary, $\Lambda z \sim 1$, where the solutions of the LSCBA for $\Lambda z = 0$ and for $\Lambda z \gg 1$ match smoothly. Notice that the exact vanishing of the density for $\Lambda z > \xi$ is an artifact of this local approximation.

The LSCBA leads to the surface density of Dirac surface states shown as a function of disorder strength Δ and for
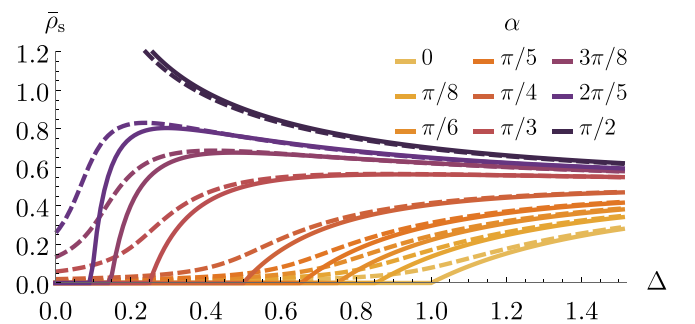

FIG. 3. Surface density of Dirac surface states ($b = 0$, solid curves) and Fermi arcs ($b = \Lambda/10$, dashed curves), as a function of disorder strength Δ, for several mixing angles between the chiral degrees of freedom $\alpha \in [0, \pi/2]$. The Dirac surface states become metallic above the critical value $\Delta_s^* = (\cos\alpha)^2$. Weyl semimetals avoid this critical point.
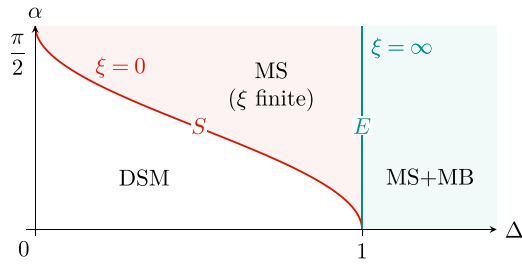
FIG. 4. Phase diagram in the (Δ, α) plane of Dirac semimetals hosting single-cone surface states (DSM). Beyond the surface critical line $S : \Delta_s^* = (\cos \alpha)^2$, metallic eigenstates populate the surface (MS). Beyond the extraordinary line $E : \Delta_b^* = 1$, the bulk becomes metallic as well (MS+MB).

various surface Fermi velocities $v_0 = \cos \alpha$ in Fig. 3. Except for nondispersing flat bands ($\alpha = \pi/2$), eigenstates do not populate the Fermi node until a critical disorder strength $\Delta_s^* = v_0^2$. This contrasts with 2D Dirac fermions, such as in graphene or the surface of 3D topological insulators in class AII where a stand-alone two-dimensional description applies due to a fully gaped bulk. There, a finite DOS develops at the nodal point under arbitrary weak disorder [64]. The difference comes from the ability of the surface states to overcome disorder by leaking through the bulk, which is prohibited in the strictly 2D case.

The corresponding phase diagram, shown in Fig. 4, resembles the one for semi-infinite spin systems [55,56], except for the absence of an ordinary transition (where the surface and the bulk develop an order parameter simultaneously). At the surface critical line $\Delta_s^*(\alpha)$, the boundary turns into a metallic state, while the bulk remains a semimetal. The bulk undergoes a transition only at $\Delta_b^* > \Delta_s^*$, when the surface is already metallic; this is known as an extraordinary transition. In addition, the surface and extraordinary critical lines merge at the special point ($\alpha = 0$, $\Delta = 1$). In contrast to spin systems, the surface transition can only exist on the boundary of three-dimensional semimetals, but not in infinite two-dimensional Dirac materials.

The group velocity also reveals a critical behavior at the surface transition. Using its definition $\boldsymbol{v} = \partial_{\boldsymbol{k}} \epsilon_s$ [49], where $\epsilon_s(\boldsymbol{k})$ denotes the surface relation dispersion, we express it as $\boldsymbol{v} = \boldsymbol{v_0}\{1 + \partial_\epsilon(\text{Re}\Sigma)[\epsilon_F(z = 0), z = 0]\}^{-1}$ at the surface nodal level, where $\boldsymbol{v_0}$ is the group velocity of the clean Dirac surface states (see the Supplemental Material [58]). We compute $\partial_\epsilon(\text{Re}\Sigma)$ by solving Eq. (5) numerically for energies ϵ around $\epsilon_F(0)$. Figure 5 shows that at surface criticality, where the dispersion relation reads $\epsilon_s \propto k^{z_s}$, the group velocity vanishes like $v \propto |\Delta - \Delta_s^*|^{\nu(z_s - 1)}$ with the surface dynamical exponent $z_s = 2$.

Effect of disorder on Fermi arcs. As shown in Fig. 3, a nonzero separation b between the surface-projected nodes generates a nonzero surface density $\bar{\rho}_s \propto b^2$ for arbitrary weak disorder. This smooths out the sharp surface transition. The
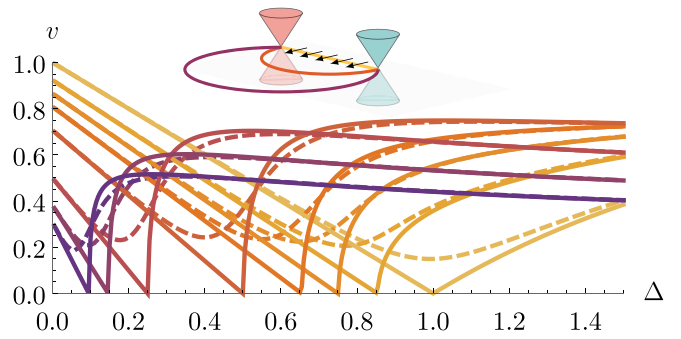

FIG. 5. Group velocity v as a function of disorder strength Δ, for several $\alpha \in [0, \pi/2]$ (see legend of Fig. 3). The solid curves are for Dirac surface states ($b = 0$); the dashed curves are for Fermi arcs ($b = \Lambda/10$). Inset: the group velocity is locally orthogonal to the arcs.

penetration length of a surface state has a minimum at the middle of the Fermi arc and is infinite at the nodal points [65]. With increasing disorder strength, the Fermi arcs broaden. The minimal penetration length grows with disorder and diverges at the extraordinary transition, which reflects dissolving of the surface states into the bulk [65]. The group velocity computed for the Fermi arc states at the junctions with the nodal points is shown in Fig. 5. It always remains finite, which also indicates that the surface transition is avoided.

Conclusion and outlook. We have studied the full phase diagram of disordered semi-infinite relativistic semimetals as a function of boundary conditions and disorder strength. To that end, we calculated the spatially resolved density of states and the surface group velocity using a local self-consistent Born approximation. We have shown that with increasing the strength of disorder, Dirac semimetals hosting single-cone surface states undergo a surface phase transition from a semimetal to a surface diffusive metal, followed by an extraordinary transition to a bulk diffusive metal. In Weyl semimetals, this surface transition is smoothed out due to the finite extension of the Fermi arcs or rays. We found that within the LSCBA, the critical exponents at the surface and special transitions equal those computed using the SCBA for the bulk transition, though we expect they differ in reality, as for the Anderson transition in semi-infinite systems [66]. We also expect the multifractality of critical surface states to deviate from that in the bulk [67,68]. Given that, we hope that our work will stimulate further analytical and numerical studies to explore our findings and refine the description of surface phenomena.

[1] S.-Y. Xu, I. Belopolski, N. Alidoust, M. Neupane, G. Bian, C. Zhang, R. Sankar, G. Chang, Z. Yuan, C.-C. Lee, S.-M. Huang, H. Zheng, J. Ma, D. S. Sanchez, B. Wang, A. Bansil, F. Chou, P. P. Shibayev, H. Lin, S. Jia, and M. Z. Hasan, Science **349**, 613 (2015).

[2] S.-Y. Xu, N. Alidoust, I. Belopolski, Z. Yuan, G. Bian, T.-R. Chang, H. Zheng, V. N. Strocov, D. S. Sanchez, G. Chang, C. Zhang, D. Mou, Y. Wu, L. Huang, C.-C. Lee, S.-M. Huang, B. Wang, A. Bansil, H.-T. Jeng, T. Neupert, A. Kaminski, H. Lin, S. Jia, and M. Z. Hasan, Nat. Phys. **11**, 748 (2015).

[3] Z. K. Liu, B. Zhou, Y. Zhang, Z. J. Wang, H. M. Weng, D. Prabhakaran, S.-K. Mo, Z. X. Shen, Z. Fang, X. Dai, Z. Hussain, and Y. L. Chen, Science **343**, 864 (2014).

[4] M. Neupane, S.-Y. Xu, R. Sankar, N. Alidoust, G. Bian, C. Liu, I. Belopolski, T.-R. Chang, H.-T. Jeng, H. Lin, A. Bansil, F. Chou, and M. Z. Hasan, Nat. Commun. **5**, 3786 (2014).

[5] S. Borisenko, Q. Gibson, D. Evtushinsky, V. Zabolotnyy, B. Büchner, and R. J. Cava, Phys. Rev. Lett. **113**, 027603 (2014).

[6] K.-Y. Yang, Y.-M. Lu, and Y. Ran, Phys. Rev. B **84**, 075129 (2011).

[7] A. A. Burkov, Nat. Mater. **15**, 1145 (2016).

[8] N. P. Armitage, E. J. Mele, and A. Vishwanath, Rev. Mod. Phys. **90**, 015001 (2018).

[9] D. T. Son and B. Z. Spivak, Phys. Rev. B **88**, 104412 (2013).

[10] L. Balents, Physics **4**, 36 (2011).

[11] X. Wan, A. M. Turner, A. Vishwanath, and S. Y. Savrasov, Phys. Rev. B **83**, 205101 (2011).

[12] Z. Wang, Y. Sun, X.-Q. Chen, C. Franchini, G. Xu, H. Weng, X. Dai, and Z. Fang, Phys. Rev. B **85**, 195320 (2012).

[13] B. Q. Lv, H. M. Weng, B. B. Fu, X. P. Wang, H. Miao, J. Ma, P. Richard, X. C. Huang, L. X. Zhao, G. F. Chen, Z. Fang, X. Dai, T. Qian, and H. Ding, Phys. Rev. X **5**, 031013 (2015).

[14] M. Z. Hasan, S.-Y. Xu, I. Belopolski, and S.-M. Huang, Ann. Rev. Cond. Mater. Phys. **8**, 289 (2017).

[15] S.-Y. Xu, C. Liu, S. K. Kushwaha, R. Sankar, J. W. Krizan, I. Belopolski, M. Neupane, G. Bian, N. Alidoust, T.-R. Chang, H.-T. Jeng, C.-Y. Huang, W.-F. Tsai, H. Lin, P. P. Shibayev, F.-C. Chou, R. J. Cava, and M. Z. Hasan, Science **347**, 294 (2015).

[16] O. Shtanko and L. Levitov, Proc. Natl. Acad. Sci. USA **115**, 5908 (2018).

[17] K. Hashimoto, T. Kimura, and X. Wu, Prog. Theor. Expt. Phys. **2017**, 053I01 (2017).

[18] Z. Faraei, T. Farajollahpour, and S. A. Jafari, Phys. Rev. B **98**, 195402 (2018).

[19] *50 Years of Anderson Localization*, edited by E. Abrahams (World Scientific, Singapore, 2010).

[20] E. Fradkin, Phys. Rev. B **33**, 3263 (1986).

[21] S. V. Syzranov and L. Radzihovsky, Ann. Rev. Cond. Mat. Phys. **9**, 35 (2018).

[22] B. Sbierski, G. Pohl, E. J. Bergholtz, and P. W. Brouwer, Phys. Rev. Lett. **113**, 026602 (2014).

[23] B. Sbierski, K. S. C. Decker, and P. W. Brouwer, Phys. Rev. B **94**, 220202(R) (2016).

[24] B. Roy, V. Juričić, and S. Das Sarma, Sci. Rep. **6**, 32446 (2016).

[25] P. Goswami and S. Chakravarty, Phys. Rev. Lett. **107**, 196803 (2011).

[26] P. Hosur, S. A. Parameswaran, and A. Vishwanath, Phys. Rev. Lett. **108**, 046602 (2012).

[27] Y. Ominato and M. Koshino, Phys. Rev. B **89**, 054202 (2014).

[28] C.-Z. Chen, J. Song, H. Jiang, Q.-f. Sun, Z. Wang, and X. C. Xie, Phys. Rev. Lett. **115**, 246603 (2015).

[29] A. Altland and D. Bagrets, Phys. Rev. Lett. **114**, 257201 (2015); Phys. Rev. B **93**, 075113 (2016).

[30] K. Kobayashi, T. Ohtsuki, K.-I. Imura, and I. F. Herbut, Phys. Rev. Lett. **112**, 016402 (2014).

[31] B. Sbierski, E. J. Bergholtz, and P. W. Brouwer, Phys. Rev. B **92**, 115145 (2015).

[32] S. Liu, T. Ohtsuki, and R. Shindou, Phys. Rev. Lett. **116**, 066401 (2016).

[33] S. Bera, J. D. Sau, and B. Roy, Phys. Rev. B **93**, 201302(R) (2016).

[34] B. Fu, W. Zhu, Q. Shi, Q. Li, J. Yang, and Z. Zhang, Phys. Rev. Lett. **118**, 146401 (2017).

[35] B. Sbierski, K. A. Madsen, P. W. Brouwer, and C. Karrasch, Phys. Rev. B **96**, 064203 (2017).

[36] S. V. Syzranov, P. M. Ostrovsky, V. Gurarie, and L. Radzihovsky, Phys. Rev. B **93**, 155113 (2016).

[37] B. Roy and S. Das Sarma, Phys. Rev. B **90**, 241112(R) (2014); see, also, Erratum **93**, 119911 (2016).

[38] T. Louvet, D. Carpentier, and A. A. Fedorenko, Phys. Rev. B **94**, 220201(R) (2016).

[39] I. Balog, D. Carpentier, and A. A. Fedorenko, Phys. Rev. Lett. **121**, 166402 (2018).

[40] T. Louvet, D. Carpentier, and A. A. Fedorenko, Phys. Rev. B **95**, 014204 (2017).

[41] B. Sbierski and C. Fräßdorf, Phys. Rev. B **99**, 020201(R) (2019).

[42] J. Klier, I. V. Gornyi, and A. D. Mirlin, Phys. Rev. B **100**, 125160 (2019).

[43] T. Holder, C.-W. Huang, and P. M. Ostrovsky, Phys. Rev. B **96**, 174205 (2017).

[44] V. Gurarie, Phys. Rev. B **96**, 014205 (2017).

[45] R. Nandkishore, D. A. Huse, and S. L. Sondhi, Phys. Rev. B **89**, 245110 (2014).

[46] J. H. Pixley, D. A. Huse, and S. Das Sarma, Phys. Rev. X **6**, 021042 (2016).

[47] J. H. Pixley, D. A. Huse, and S. Das Sarma, Phys. Rev. B **94**, 121107(R) (2016).

[48] J. H. Wilson, J. H. Pixley, P. Goswami, and S. Das Sarma, Phys. Rev. B **95**, 155122 (2017).

[49] J. H. Wilson, J. H. Pixley, D. A. Huse, G. Refael, and S. Das Sarma, Phys. Rev. B **97**, 235108 (2018).

[50] K. Ziegler and A. Sinner, Phys. Rev. Lett. **121**, 166401 (2018).

[51] M. Buchhold, S. Diehl, and A. Altland, Phys. Rev. Lett. **121**, 215301 (2018).

[52] M. Buchhold, S. Diehl, and A. Altland, Phys. Rev. B **98**, 205134 (2018).

[53] R.-J. Slager, V. Juričić, and B. Roy, Phys. Rev. B **96**, 201401(R) (2017).

[54] A. Sinner and K. Ziegler, Phys. Rev. B **96**, 165140 (2017).

[55] T. C. Lubensky and M. H. Rubin, Phys. Rev. B **12**, 3885 (1975).

[56] T. C. Lubensky and M. H. Rubin, Phys. Rev. B **11**, 4533 (1975).

[57] H. Nielsen and M. Ninomiya, Phys. Lett. B **105**, 219 (1981).

[58] See Supplemental Material at http://link.aps.org/supplemental/10.1103/PhysRevB.103.L081405 for the explicit form of the

Green's functions, derivation of LSCBA, and calculation of group velocity.

[59] E. Witten, Riv. Nuovo Cim. **39**, 313 (2016).

[60] Z. Faraei and S. A. Jafari, Phys. Rev. B **100**, 035447 (2019).

[61] S.-Y. Xu, I. Belopolski, D. S. Sanchez, C. Zhang, G. Chang, C. Guo, G. Bian, Z. Yuan, H. Lu, T.-R. Chang, P. P. Shibayev, M. L. Prokopovych, N. Alidoust, H. Zheng, C.-C. Lee, S.-M. Huang, R. Sankar, F. Chou, C.-H. Hsu, H.-T. Jeng, A. Bansil, T. Neupert, V. N. Strocov, H. Lin, S. Jia, and M. Z. Hasan, Sci. Adv. **1**, e1501092 (2015).

[62] H. Inoue, A. Gyenis, Z. Wang, J. Li, S. W. Oh, S. Jiang, N. Ni, B. A. Bernevig, and A. Yazdani, Science **351**, 1184 (2016).

[63] M. Papaj, H. Isobe, and L. Fu, Phys. Rev. B **99**, 201107(R) (2019).

[64] P. M. Ostrovsky, I. V. Gornyi, and A. D. Mirlin, Phys. Rev. B **74**, 235443 (2006).

[65] E. V. Gorbar, V. A. Miransky, I. A. Shovkovy, and P. O. Sukhachov, Phys. Rev. B **93**, 235127 (2016).

[66] A. R. Subramaniam, I. A. Gruzberg, A. W. W. Ludwig, F. Evers, A. Mildenberger, and A. D. Mirlin, Phys. Rev. Lett. **96**, 126802 (2006).

[67] E. Brillaux, D. Carpentier, and A. A. Fedorenko, Phys. Rev. B **100**, 134204 (2019).

[68] S. Syzranov, V. Gurarie, and L. Radzihovsky, Ann. Phys. **373**, 694 (2016).